Macromolecules
ARTICLE

Macromolecules **2010**, *43*, 9131–9138 **9131**
DOI: 10.1021/ma101252c

Molecular Simulation Study of the Structure of High Density Polymer Brushes in Good Solvent

Ian G. Elliott, Tonya L. Kuhl, and Roland Faller*

Department of Chemical Engineering and Materials Science, University of California at Davis, Davis, California, 95616

Received June 4, 2010; Revised Manuscript Received September 10, 2010

ABSTRACT: Molecular dynamics simulations are presented of coarse-grained, polar, polymer brushes in a good polar solvent at high grafting densities. Chain extension is heavily influenced by temperature, stretching far from the surface at high temperature (350 K) while weak absorption and loop formation is observed at low temperature (300 K). Simulations of isolated free chains of different lengths in solution demonstrate the polymers are in good solvent conditions at both temperatures. Consistent with previous findings, increasing grafting density leads to larger chain extension under all conditions. A saturation limit at about half the bulk polymer density is found for high chain length and grafting density. Even at very high grafting densities a polymer depletion region near the surface is observed at 350 K due to an orthogonal orientation of the chain at the grafting surface. Radial distribution functions reveal that the grafting pattern does not affect the overall brush configuration beyond the first five monomers of each chain as long as the surface is homogeneously covered.

1. Introduction

A polymer brush is formed when solvated polymer chains are grafted to a surface at a density high enough that they laterally interact with each other. Excluded volume effects and the affinity of the polymer to the solvent cause the chains to stretch away from the surface.[1] Polymer brushes have been studied extensively due to their ability to modify surface properties, prevent colloid aggregation, and enhance lubrication or adhesion.[2−5] When properly designed, polymer brushes in good solvent conditions have been shown to remarkably reduce friction.[6] The brush structure and its properties can be controlled by tuning grafting density, polymer molecular weight, temperature, and solvent quality.[7] In order to design polymer brushes effectively for specific applications, it is necessary to understand how the system is affected by these variables. Numerous theoretical,[8−15] experimental,[16−20] and simulation[21−34] studies have examined polymer brush structure and properties, yet most of these have not investigated brushes at very high grafting densities.

Molecular simulations are excellent tools for studying polymer brush systems under varying conditions. Many conditions are difficult or impossible to examine with physical experiments; thus, simulations can provide insight into features of the system that cannot otherwise be accessed and understood. Simulation data corresponding to specific experimental conditions can be compared to validate or modify the simulation model. For this work, a polar polymer brush system in a good, polar solvent was simulated using a coarse-grained approach. All nonbonded interactions are based on a Lennard-Jones potential. The surface has an attractive interaction with both the polymer and solvent although not as strong as polymers and solvents among each other. The simulations represent roughly 3000−10 000 g/mol chains (40−150 coarse-grained monomers) over a range of grafting densities. Coarse-graining is necessary to enable reasonable polymer lengths to be reached, while still allowing for high grafting densities. The high grafting densities examined in this study are achievable experimentally by "grafting from" techniques such as atomic transfer radical polymerization (ATRP).[35,36] For such systems, atomistic simulations are not feasible due to both the large number of particles and the ensuing long equilibration times.

*Corresponding author. E-mail: rfaller@ucdavis.edu.

2. Model

Coarse-grained molecular dynamics simulations were performed based on the MARTINI lipid model (V 1.4) developed by Marrink.[37] This model has been successfully used to study amphiphilic copolymer systems interacting with surfaces[38] and polymer brush systems.[39] To increase polymer chain length and the efficiency of the simulation, every interaction site represents 4−5 heavy atoms as one "superatom". Each superatom is set to a mass of 72 amu, corresponding for example, to the mass of four water molecules. This mass is not intended to reproduce a specific polymer, but instead is representative of a generic polar polymer. One example of a coarse-grained mapping is shown in Figure 1 where water and polyethylene-oxide (PEO) are used to exemplify the model. Using such a representation, the effect of variables such as grafting density, chain length, and temperature on the brush structure can be qualitatively determined for systems that are too large for atomistic simulations. It should be noted, however, that specifics of the water−poly(ethylene oxide) system cannot be deduced from these coarse-grained simulations. Instead, the properties of a generic polar solvent−polar polymer brush system are examined.

In the model, superatoms along the polymer backbone interact by a weak harmonic potential based on an equilibrium bond length (R_{bond}) of 0.47 nm and a force constant (K_{bond}) of 1250 kJ mol^{-1} nm^{-2}.

$$V_{bond}(R) = \frac{1}{2} K_{bond}(R - R_{bond})^2 \quad (1)$$

R is the distance between a bonded pair. Similarly, angle bending is described with a weak cosine based angle potential with an equilibrium bond angle (θ_0) of 180° and a force constant (K_{angle}) of 25 kJ mol^{-1} rad^{-2}.

$$V_{angle}(\theta) = \frac{1}{2} K_{angle}[\cos(\theta_0) - \cos(\theta)]^2 \quad (2)$$

θ is the angle between three consecutive superatoms. The weak bonding potentials yield a flexible polymer chain. Nonbonded

Published on Web 10/07/2010

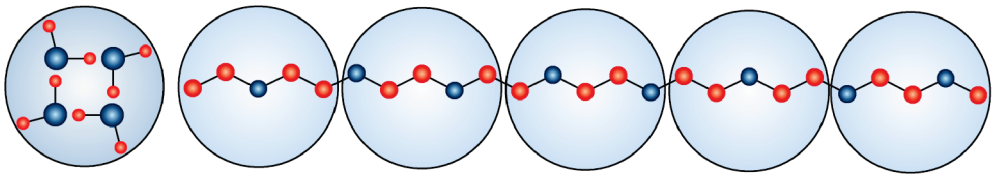

Figure 1. Coarse-grained representations for superatoms of solvent, e.g., water (left), and polymer, e.g., PEO (right). Each coarse-grained superatom has a mass of 72 amu, representing 4−5 heavy atoms.

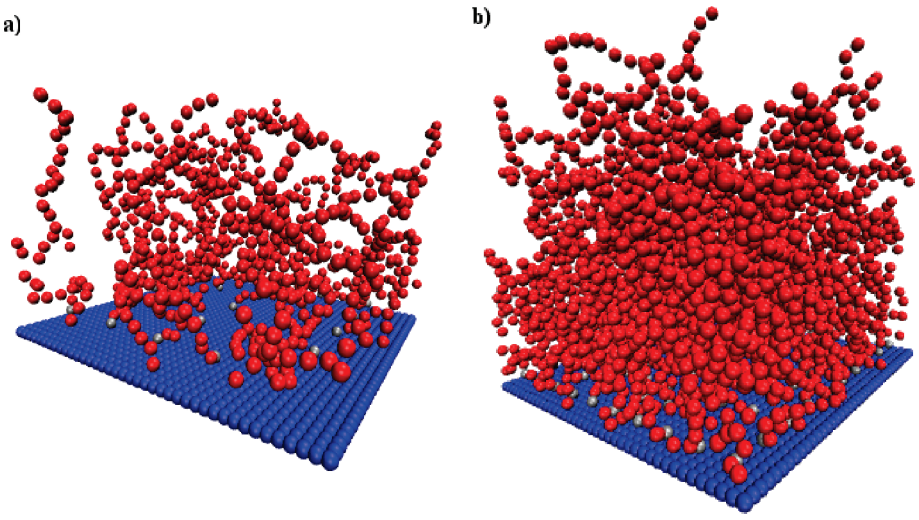

Figure 2. Snapshots using the VMD package[40] of the lowest (a) and highest (b) grafting density brush systems of 40 monomer chains at 350 K. Polymer atoms are red, surface atoms are blue, and chain grafting sites are silver. Solvent particles are omitted for clarity.

interactions are represented by a Lennard-Jones potential.

$$V_{\mathrm{LJ}}(\mathrm{r}) = 4\varepsilon\left[\left(\frac{\sigma}{r}\right)^{12} - \left(\frac{\sigma}{r}\right)^{6}\right] \tag{3}$$

r is the particle separation distance, σ represents the range of the interaction, and ε the interaction strength. Lennard-Jones interactions, which are not considered for directly bonded particles, account for interactions of particles that are generically polar, nonpolar, or charged in the MARTINI model. Therefore, this model does not describe a specific polymer−solvent system. It instead can be used to represent a polar or nonpolar brush system in good, Θ, or poor solvents. For these studies, a polar polymer in a good, polar solvent was simulated. When using this coarse-grained model there is an inherent speed up of the dynamics by a factor of 4 and simulation times are often multiplied by 4 to reflect this.[37] All times reported in this paper are the actual simulation times and not the effective times, accounting for the increase in dynamics.

Particles that compose the surface remained completely fixed throughout the simulation and only interacted with moving particles. The surface was infinitely extended through periodic boundary conditions in the $x-y$ plane, and prevented particles from passing through. Polymer chains were grafted to the surface in a regular pattern. When possible a square grid was used (e.g., 25 chains grafted as five rows with five equally spaced chains each). If a square grid was not possible, the closest square was used with additional chains inserted and the in-plane distances within the augmented rows and columns were adapted to distribute chains evenly. One end monomer of each polymer chain was fixed 0.3 nm above the surface, creating an end-grafted system as shown in Figure 2. As with the polymer and solvent, the surface was polar. The surface interaction with the solvent and polymer chains was reduced to about one-third the interaction between all other polar particles to mitigate polymer adsorption to the surface. The Lennard-Jones values for each particle interaction are provided in Table 1.

Gromacs versions 3.3.3[41] or 4.0.4[42] were used for the simulations. Orthorhombic periodic boundary conditions were applied in all three dimensions. The box was 12 nm long in the x and y directions. The z direction length was selected to be larger than the length of a fully stretched chain plus the interaction cutoff radius. The z length was thus different for each chain length, and ranged from about 20 to 80 nm. Semi-isotropic pressure coupling was invoked, fixing the box length in the x and y direction and allowing the z direction to vary, maintaining the normal pressure at 1 atm. The z direction length typically changed less than 2 nm throughout the course of the simulation due to pressure coupling. A Berendsen barostat[43] was used for pressure coupling with a correlation time $\tau_{\mathrm{P}} = 1$ ps when using Gromacs 3.3.3 and $\tau_{\mathrm{P}} = 2$ ps when using Gromacs 4.0.4. Temperature was controlled using a Berendsen thermostat[43] with a correlation time of $\tau_{\mathrm{T}} = 1$ ps.

A steepest decent energy minimization algorithm was used to remove initial bad contacts created by placing atoms in the box. To stabilize the system further, the first nanosecond of each simulation used a small time step of 0.001 ps. Following this stabilization the simulation proceeded with a time step of 0.02 ps. A Verlet-type neighbor list was used and updated every 10 steps with a 1.2 nm cutoff with the twin-range cutoff method.[44] The Lennard-Jones cutoff distance was $r_{\mathrm{cut}} = 1.2$ nm.

3. Systems

A polar polymer brush system in good solvent was examined under equilibrium conditions. Polymer brush properties were characterized at different grafting densities, temperatures, and chain lengths. The grafting densities studied were 0.174, 0.347,

0.486, and 0.694 chains/nm^2, the highest of which corresponds to the upper limit experimentally attainable with "grafting from" approaches such as ATRP.[45] Simulations at all grafting densities were performed for chains of 40 coarse-grained monomers at 300 and 350 K. All grafting densities were additionally studied using longer chains of 100 coarse-grained monomers at 350 K. The highest grafting density was further investigated with chains of 150 monomers at 350 K. Often grafting density is expressed as an overlap grafting density[36,46,47] defined by

$$\sigma^* = \pi R_g^2 \Sigma \quad (4)$$

where Σ is the grafting density expressed as chains/area and R_g is the radius of gyration obtained from simulations of an isolated free polymer chain in solution. The overlap grafting density represents the ratio of the cross sectional area the chains would adopt in a free solution to the area the chains have per grafted site in the brush. When $\sigma^* < 1$, the system is considered to be in the mushroom regime where the chains do not have significant lateral interaction. For $\sigma^* > 1$, the chains are restricted to less area than they would occupy in solution, and therefore interact with neighboring chains forming a brush. σ^* in this study ranged from modest ($\sigma^* = 3.48$) to very high ($\sigma^* = 71.4$). The specifics of all systems are given in Table 2.

Table 1. Lennard-Jones Interaction Parameters for each Coarse-Grained Particle Type

interaction	σ (nm)	ε (kJ/mol)
solvent−solvent	0.47	5.00
polymer−polymer	0.47	5.00
polymer−solvent	0.47	5.00
wall−polymer	0.47	1.68
wall−solvent	0.47	1.68

Table 2. Details for All Simulations[a]

grafting density, Σ (chains/nm^2)	σ^*	monomers per chain	temperature (K)	total simulation time (ns)	production time (ns)
0.174	3.85	40	300	5000	3000
	3.48	40	350	1100	1000
	9.87	100	350	2000	1500
0.347	7.71	40	300	800	500
	6.97	40	350	1300	1100
	19.7	100	350	8700	3700
0.486	10.8	40	300	5100	3100
	9.75	40	350	1300	1000
	27.6	100	350	6002	5002
0.694	15.4	40	300	6200	3000
	13.9	40	350	1400	1200
	39.5	100	350	6192	3192
	71.4	150	350	4292	1792

[a] Production time is the amount of time that reported properties were averaged over after equilibration.

4. Results

For a polymer system, the longest relaxation time is the chain reorientation time. Therefore, this property was monitored to confirm equilibration. Rotational autocorrelation functions accounted for the reorientation of a vector defined between the first and last monomers of a polymer chain. For a polymer melt or solution where the chains are able to freely move, the system would be considered equilibrated once the rotational autocorrelation function reached zero. A polymer brush system, however, has chains attached at the surface, which imposes an orientation on the chains throughout the simulation and thus the autocorrelation function never reaches zero. Therefore, for the brush systems examined, equilibrium was defined as the point when the autocorrelation function reaches a steady, long time limit. Depending heavily on chain length, equilibration took anywhere from 100 ns to several microseconds to achieve (see Table 2). The rotational autocorrelation functions for the lower temperature and longer chain systems showed greater variability compared to the 40 monomer chains at 350 K. Equilibrium was additionally confirmed for the low temperature and long chain systems by observing negligible change in the polymer density profile and the radius of gyration over several hundred nanoseconds. In the following, all reported property averages were taken after the system had equilibrated.

At 300 K, surface adsorption dominated over excluded volume stretching for all grafting densities. The chains adsorbed to the surface until roughly a monolayer was formed, and extended only weakly into the solvent as indicated in Figure 3. Density profiles for 350 K simulations at the same grafting densities are also shown in the plot in Figure 3a to clearly illustrate the influence of temperature. In addition, Figure 4 shows the increase in extension from the surface at 350 K with increasing grafting density for chain lengths of 40, 100, and 150 monomers. The 300 K simulations were initialized with the output configuration from the 350 K runs and thus began stretched. As each low temperature simulation adsorbed from a stretched state, the final structures should be viewed as the equilibrium structure and not as the conformation of a brush in a kinetic trap.

The difference between the brush structure at 300 and 350 K raises the question of solvent quality. Simulations of isolated ungrafted polymers in solution were conducted at several chain lengths ranging from 20 to 150 monomers at both 300 and 350 K to ascertain how the solvent quality depended on temperature. The radius of gyration data is shown in Figure 5a for 300 K and Figure 5b for 350 K. A power law is fit to each set of data to determine the dependence of radius of gyration on chain length.

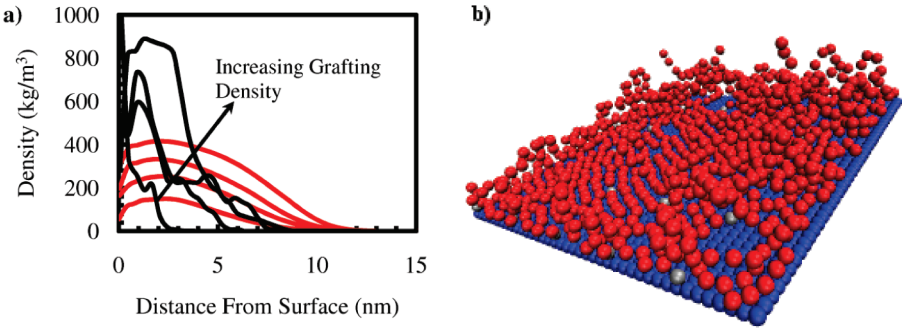

Figure 3. (a) Polymer density profiles of a brush consisting of 40 monomer chains at four grafting densities (Σ = 0.174, 0.347, 0.486, and 0.694 chain/nm^2) at 300 K (black) and 350 K (red). Grafting density increases from bottom to top for both black and red curves. (b) A VMD[40] image corresponding to the lowest grafting density system of Σ = 0.174 chains/nm^2 of 40 monomer chains at 300 K.

This dependence is compared to the theoretical prediction of $R_g \sim N^{\nu}$ where $\nu = 0.5$ and 0.6 for Θ and good solvents, respectively. As ν in each case is close to 0.6, all simulations at 300 and 350 K were conducted in good solvent conditions although at 300 K a slight tendency toward Θ conditions was observed ($\nu = 0.55$). The polymer adsorption observed at 300 K was therefore not due to poor solvent quality, but instead resulted from adsorption to the surface which often created chain loops. In the case of low grafting densities, most of the polymer is adsorbed in the monolayer above the surface. At higher grafting densities, a monolayer is still adsorbed to the surface, but many of the chains adsorb at segments in the middle or end of the chain, forming loops as shown in Figure 6. Loops of this sort were observed for $\Sigma = 0.347$, 0.486, and 0.694 chains/nm^2 and were not present for the lowest grafting density as too many of the chains were adsorbed to allow for loops as in Figure 3b. This restriction accounts for the double peaks observed in the 300 K density profiles in Figure 3. Essentially there are two populations of chains with very different dimensions. One group forms loops or adsorbed chains, yielding a shorter brush height than expected for good solvent conditions. The second does not adsorb, as no adsorption sites are vacant, and stretches out into the solvent from excluded volume interactions as shown in Figure 6. The effect is the density profile exhibits one peak close to the surface from the loops, and a smaller peak farther away from the surface corresponding to the stretched chains. There are of course situations in between the two extremes shown in Figure 6, where the chains partially adsorb or form a loop near the bottom of the chain, and then extend outward from the surface. This simply broadens the peaks in the density profiles and makes the second peak less noticeable.

Another interesting difference of the profiles with respect to temperature is observed very close to the surface. As the temperature increases from 300 to 350 K (Figure 3), the absorbed layer of polymer vanishes completely and a solvent-rich polymer depletion layer forms. This effect is even more obvious in the solvent density profiles for varying polymer grafting densities presented in Figure 7.

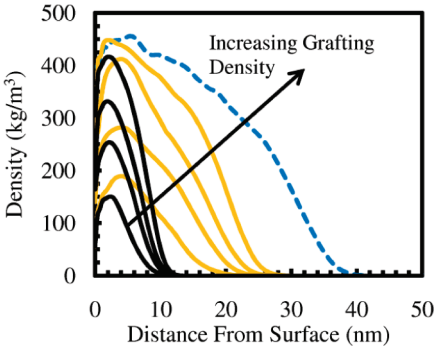

Figure 4. Polymer density profiles of polymer brushes at different grafting densities at 350 K. Data is presented for chains of 40 (solid black), 100 (solid orange), and 150 (dashed blue) monomers.

For all grafting densities at 350 K, a peak occurs in each solvent density profile near the surface indicating a polymer depletion layer. The depletion region is due to the surface limiting the chain orientations that can be adopted close to the surface, reducing their entropy. This has been observed for low grafting densities previously[48−50] but was not expected for high grafting densities as the entropic penalty for chain extension decreases with increasing grafting density or chain length. A depletion layer for high grafting densities has rarely been reported.[29,30]

The structural dependence of the brush with respect to chain length was also examined. Focusing on the highest grafting density curves of Figure 4 at chain lengths of 40, 100, and 150 monomers, the influence of chain length at high grafting density can be deduced. A plateau in the density profile occurred at around 450 kg/m^3. Increasing the chain length by 50% from 100 to 150 monomers did not significantly increase the maximum polymer density, but rather broadened the curve through greater chain extension. Therefore, once the peak polymer density reached about half the bulk density, increasing the chain length caused further chain extension away from the surface as opposed to increasing the amount of polymer near the surface. The numerical value for the maximum brush density is assumed to be model dependent. However, the concept of a maximum density is not. In these simulations, a plateau was reached with a grafting density of 0.694 chains/nm^2, but not for any lower grafting densities. Thus, the critical grafting density for saturation is between 0.486 and 0.694 chains/nm^2. A flattening out of the density profile has been reported for large σ^* values in other simulation studies.[30,31]

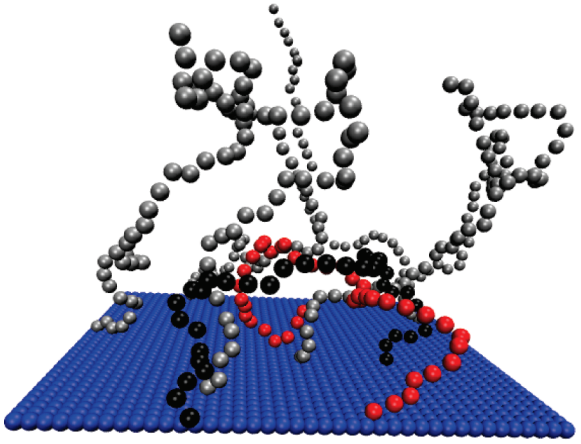

Figure 6. Snapshot of selected chains from a brush system at 300 K with grafting density $\Sigma = 0.694$ chains/nm^2 and $N = 40$. Two chains that form loops (red and black) by having monomers near their ungrafted ends adsorb to the surface are shown. Several stretched chains are present (silver) to illustrate the different conformations occurring at the lower temperature.

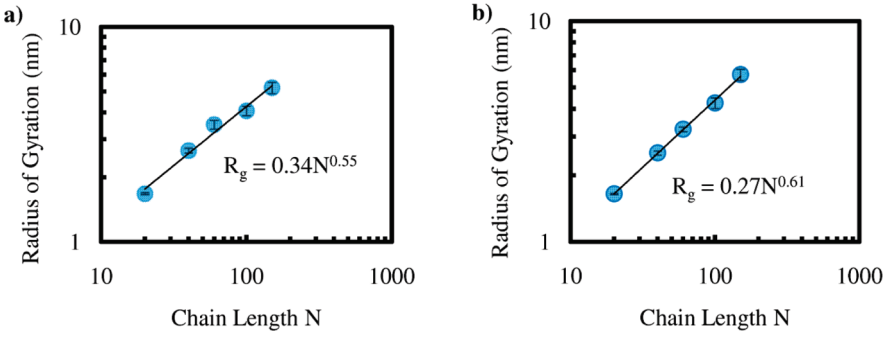

Figure 5. Radius of gyration versus chain length data for simulations of isolated, free chains in solution at (a) 300 K and (b) 350 K.

The polymer chain end distribution was calculated for the 350 K systems by using the density profile of each chain's end monomer and normalizing it to a total probability of unity (Figure 8). In all cases, the chain end has a finite probability of being at the surface. The peak in the end distribution profile is shifted away from the surface when either grafting density or chain length is increased. Self-consistent field theory[1,9] predicts the peak to occur at $z = 0.7h_0$. The simulated density profiles are close to this peak value for all but the lowest grafting density.

The average chain tilt was calculated to quantify the brush orientation with respect to the surface. A vector was defined for each polymer chain from the grafting site to the free end monomer and the angle between this vector and the surface normal defined the tilt. Smaller tilt angles indicate a chain orientation more normal to the surface. Tilt as a function of overlap grafting density is provided in Figure 9a and yields an almost linearly decreasing tilt with overlap grafting density. To explicitly show the effect of chain length, tilt is also plotted against grafting density for different chain lengths in Figure 9b. The average chain tilt substantially decreased with either grafting density or chain length. The lowest average angle was observed for the highest grafting density and chain length, indicating an increased orientation normal to the surface (i.e., greater extension from the surface).

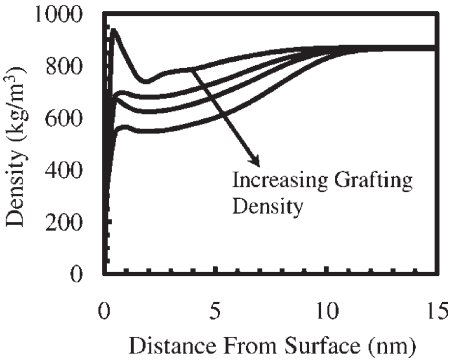

Figure 7. Solvent density profiles corresponding to polymer brush systems comprised of 40 monomer chains at 350 K for different grafting densities.

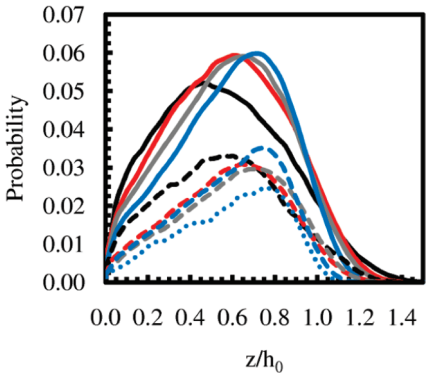

Figure 8. Chain end distributions of polymer brushes at 350 K in good solvent. Grafting densities are $\Sigma = 0.174, 0.347, 0.486$, and 0.694 chains/nm^2 represented by black, red, gray, and blue lines, respectively. Chain lengths are $N = 40$, 100, and 150 monomers represented with solid, dashed, and dotted lines, respectively.

The uncompressed brush height is another useful quantity from simulation results that can be compared to theoretical models. Following the work of Binder's group[32,33] brush height was defined as

$$h_0 = \frac{8}{3}\langle z \rangle = \frac{8}{3}\frac{\int_0^\infty z\phi(z)\,dz}{\int_0^\infty \phi(z)\,dz} \quad (5)$$

where $\phi(z)$ is the polymer density profile and z is the distance from the surface.

This value was normalized by chain length and compared to theoretical models predicting the dependence of brush height on grafting density. Theoretically, for a single brush in good solvent the brush height is expected to scale as $h_0/N \sim \sigma^{*1/3}$ where h_0 is the uncompressed brush height, N the number of monomers per chain, and σ^* the overlap grafting density.[14,46] Figure 10 depicts the simulated brush height values as a function of overlap grafting density with a power law fit to compare to theory.

While Figure 10 was expected to yield a universal curve, two distinct trends were observed depending on chain length. The 40 and 100 monomer chain data scale as $\sigma^{*0.14}$ and $\sigma^{*0.25}$ respectively. Increasing chain length pushes the trend toward the theoretically predicted $\sigma^{*0.33}$. As self-consistent mean field theory becomes more reliable with increasing chain length, it is expected that data for the 150 monomer chains would follow the theoretical trend more

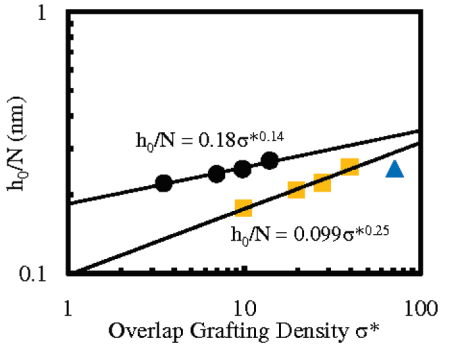

Figure 10. Values of uncompressed brush height normalized by chain length versus overlap grafting density. Three different chain lengths of 40 monomers (black circles), 100 monomers (orange squares), and 150 monomers (blue triangles) are shown.

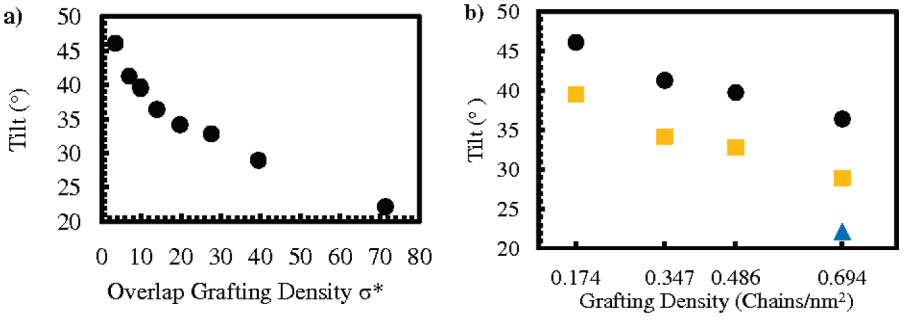

Figure 9. Average tilt angle of polymer chains at 350 K as a function of overlap grafting density (a) and grafting density (b). In part b, data are given for three different chain lengths of 40 (black circles), 100 (orange squares), and 150 (blue triangles) monomers. Tilt is defined as the angle between the surface normal and a vector from the grafting site to the end monomer of each chain.

closely. Experimentally, however, deviations from the theoretical trend have been reported. Kent[51] found brush height varying as $\sigma^{*0.22}$ for good solvent, which is quite close to the trend for the longer chains in Figure 10.

Similar to eq 5, the root-mean-squared (rms) brush height can be defined as,[46,52]

$$h_{\mathrm{rms}}{}^2 = \frac{\int_0^\infty z^2\phi(z)\,\mathrm{d}z}{\int_0^\infty \phi(z)\,\mathrm{d}z} \tag{6}$$

For good solvent, analytical self-consistent field theory (ASCF)[46,52] predicts parabolic density profiles where the root mean squared brush height values relate to the brush height as $h^0_{\mathrm{rms}} = h_0/\sqrt{5}$. The brush heights in this study follow this relation nearly perfectly (see Table 3), with the good solvent ASCF predicted h^0_{rms} values deviating by less that 0.5% of the calculated h^0_{rms} for all systems at 350 K. A similar relationship exists for Θ solvents, predicting $h^0_{\mathrm{rms}} = h_0/2$. The ASCF Θ solvent prediction deviates significantly from the calculated h^0_{rms} values in this work. Along with the free chain radius of gyration data, this additionally confirms that the simulations conducted at 350 K were in good solvent conditions. Table 3 indicates that, although the chains are short in comparison to the long chains of self-consistent field theory, the ratios predicted are nonetheless applicable as they depend very weakly on chain length.

Table 3. Comparison of the Simulated h^0_{rms} Values to Theoretical Predictions for Good and Θ Solvents Based on h_0

			h^0_{rms} (nm)		
				ASCF	
monomers per chain	grafting density, Σ (chains/nm^2)	h_0 (nm)	simulated good solvent	good solvent	Θ solvent
40	0.174	8.852	3.957	3.959	4.426
	0.347	9.603	4.305	4.295	4.802
	0.486	10.032	4.496	4.486	5.016
	0.694	10.812	4.835	4.835	5.406
100	0.174	17.77	7.905	7.947	8.885
	0.347	20.889	9.333	9.342	10.445
	0.486	22.182	9.962	9.920	11.091
	0.694	25.591	11.407	11.445	12.796
150	0.694	37.696	16.810	16.858	18.848

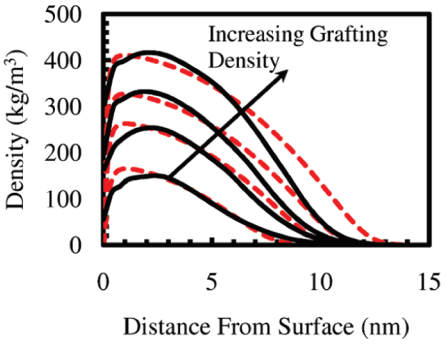

Figure 11. Polymer density profiles from simulations (solid black) and numerical self-consistent field theory (dashed red) at grafting densities of (from bottom to top) Σ = 0.174, 0.347, 0.486, and 0.694 chains/nm^2.

To further compare the simulated results with theoretical predictions, calculations were performed using the numerical self-consistent field (NSCF) theory model developed by Whitmore et al.[46] using the same conditions as in the simulations. Figure 11 presents simulated density profiles for 40 monomer chains at 350 K for the four grafting densities studied and compares them to profiles produced using NSCF theory with parameters $N = 40$, $b = 0.47$ nm, $l = 0.157$ nm, $\chi = -1.25$, $\rho_{0A} = 0.85b^{-3}$, and $\rho_{0S} = 0.75b^{-3}$. NSCF profiles were also examined for $\chi = 0$ and 0.4, but both of these yielded results that significantly deviated from the simulations.

The predictions from NSCF theory match the simulation results relatively well considering the short chain lengths. The primary difference is that NSCF theory predicts a smaller polymer depletion region as the peak occurs closer to the surface. NSCF theory also predicts larger chain extension than was observed for the higher grafting densities.

Radial distribution functions $g(r)$ were calculated to investigate lateral order within the brush and to determine how grafting patterns influence the structure. Reflecting the two-dimensional nature of the system, the radial distribution functions were calculated within the $x-y$ plane for a given set of atoms in the polymer chains. A specific monomer in each chain was considered, and its correlation with respect to the same monomer in all other chains determined. For low grafting density, peaks were observed in the radial distribution function that directly corresponded to the applied grafting pattern. These peaks are most pronounced for the monomers close to the grafting point, and dissipate by about the fifth monomer as shown in Figure 12a. Radial distribution functions for the highest grafting density in Figure 12b indicate correlations at intervals corresponding to the bead size (0.47 nm) up to two layers away. For monomers at the base of the chain, there are also peaks corresponding to the grafting pattern, but this quickly vanishes except for the nearest neighboring chain. Therefore, at low grafting density the grafting pattern only influenced the chain segments closest to the surface. For high grafting density systems, correlations were observed

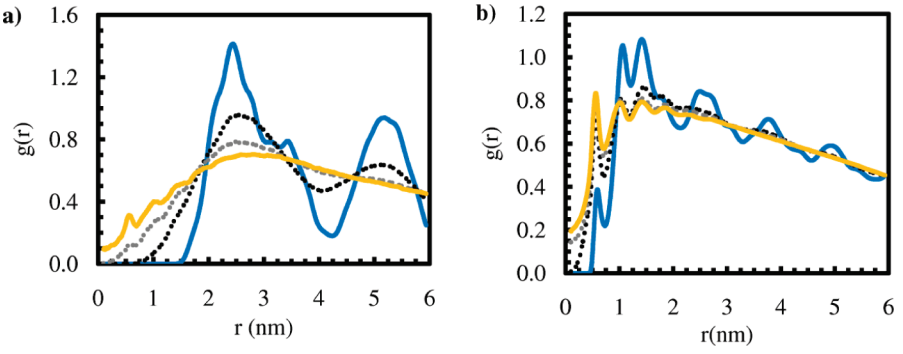

Figure 12. Lateral radial distribution functions of specific monomers in a polymer brush. The brush consists of chains of 40 monomers at 350 K grafted at the lowest grafting density of 0.174 chains/nm^2 (a) and the highest grafting density of 0.694 chains/nm^2 (b). Data are given for the correlation between the second (solid blue), third (dotted black), fourth (dotted gray), and fifth (solid orange) monomers from the grafting site. A running average was taken over the data such that each data point is averaged over about 0.1 nm.

between nearest neighboring chains throughout most of the brush. These correlations are due to the fact that it is a densely packed brush, and as such, correlations with neighboring particles are inevitable. Therefore, the grafting pattern used (regular or random) does not affect the overall structure of the brush provided the grafting density heterogeneity is not significant.

5. Conclusion

Polymer brushes were characterized with respect to grafting density, temperature, and molecular weight. A coarse-grained representation of a polar polymer in polar solvent was used to obtain qualitative structure information on the system. Static properties such as density profiles, radial distribution functions, chain tilt, and brush height were used to quantify brush structure. High grafting densities up to $\Sigma = 0.694$ chains/nm^2 or $\sigma^* = 71.4$ were examined.

Temperature substantially affected brush structure, dictating whether adsorption to the surface or chain extension dominates. Lower temperature favored surface adsorption, while higher temperature led to greater chain extension. Determination of the single chain radius of gyration at various chain lengths demonstrated that both the 300 and 350 K simulations were conducted under good solvent conditions. Brush height relations between h_0 and h^0_{rms} were also found to be consistent with good solvent predictions. The structure of the 300 K brushes as determined by density profiles resembled a collapsed brush in poor solvent conditions. This was not the case, however. Upon closer inspection of the trajectories, the collapsed structure was attributed to the formation of absorbed loops. Chains which did not form loops extended from the surface normally for a good solvent.

Grafting density strongly affected the structure of the brush. Higher grafting densities and their correspondingly higher excluded volume interactions caused greater chain extension from the surface at all temperatures and chain lengths. This was additionally confirmed by the average chain tilt relative to the surface which demonstrated that chains oriented more normal to the surface with increasing grafting density or chain length. In addition, the presence of the surface and resulting configurational entropy loss of chain ends close to the surface also contributed to the normal orientation of the chains. As a result, in all 350 K simulations a polymer depletion region was observed near the grafting surface even at the very high grafting densities studied. Increasing chain length led to an increase in the maximum polymer density and chain extension for the three lower grafting densities studied. The highest grafting density system eventually reached a saturation limit, and therefore only chain extension was affected by polymer length after this limit was reached. This should be a general feature for all polymer−solvent systems and provide a limit on the maximum density of polymer near the surface.

Lateral radial distribution functions indicate that the grafting pattern only substantially affected the first five monomers from the surface on each chain. Beyond that, there was little order between chain segments corresponding to the grafting site separation, and thus the grafting pattern was essentially lost. Similar results may therefore be expected for systems formed with a regular or random grafting pattern, provided the grafting points are reasonably distributed on the surface.

With static properties understood, similar studies will be conducted to examine the system's dynamic response to perturbation such as shear and compression. Polydispersity, which has been shown to greatly affect brush structure particularly at high grafting densities,[53] will also be investigated.

The structure of the adsorbed polymers at the surface may be influenced by kinetic traps whereas the simulations overall are definitely in equilibrium. In order to address the structure of the adsorbed layer advanced Monte Carlo moves may be helpful.

Acknowledgment. This work was supported by the United States Department of Energy, Office of Basic Energy Science, under Grant DE-FG02-06ER46340. I.G.E. additionally thanks the Graduate Assistance in Areas of National Need (GAANN) program of the US Department of Education. Computer time at the National Energy Research Supercomputer Center, which is supported by the Office of Science of the U.S. Department of Energy under Contract No. DE-AC03-76SF00098, has been used for parts of the simulations.

References and Notes

(1) Milner, S. T. *Science* **1991**, *251* (4996), 905–914.
(2) Advincula, R. C.; Brittain, W. J.; Caster, K. C.; Ruhe, J., *Polymer Brushes*; Wiley-VCH: Weinheim, Germany, 2004.
(3) Napper, D. H. *Polymeric Stabilization of Colloidal Dispersions*; Academic Press: London, 1983.
(4) Hamilton, W. A.; Smith, G. S.; Alcantar, N. A.; Majewski, J.; Toomey, R. G.; Kuhl., T. L. *J. Polym. Sci., Part B: Polym. Phys.* **2004**, *42* (17), 3290–3301.
(5) Pastorino, C.; Binder, K.; Kreer, T.; Muller, M. *J. Chem. Phys.* **2006**, *124* (6), 064902.
(6) Klein, J.; Kumacheva, E.; Mahalu, D.; Perahia, D.; Fetters, L. J. *Nature* **1994**, *370* (6491), 634–636.
(7) Auroy, P.; Auvray, L.; Léger, L. *Phys. Rev. Lett.* **1991**, *66* (6), 719.
(8) Alexander, S. *J. Phys.* **1977**, *38*, 983.
(9) Milner, S. T.; Witten, T. A.; Cates, M. E. *Macromolecules* **1988**, *21* (8), 2610–2619.
(10) Milner, S. T.; Witten, T. A.; Cates, M. E. *EPL* (*Europhys. Lett.*) **1988**, *5* (5), 413–418.
(11) Halperin, A.; Zhulina, E. B. *Macromolecules* **1991**, *24* (19), 5393–5397.
(12) Biesheuvel, P. M. *J. Colloid Interface Sci.* **2004**, *275* (1), 97–106.
(13) Biesheuvel, P. M.; de Vos, W. M.; Amoskov, V. M. *Macromolecules* **2008**, *41* (16), 6254–6259.
(14) de Gennes, P. G. *Macromolecules* **1980**, *13* (5), 1069–1075.
(15) Wijmans, C. M.; Scheutjens, J. M. H. M.; Zhulina, E. B. *Macromolecules* **1992**, *25* (10), 2657–2665.
(16) Auroy, P.; Mir, Y.; Auvray, L. *Phys. Rev. Lett.* **1992**, *69* (1), 93.
(17) Cho, J.-H. J.; Smith, G. S.; Hamilton, W. A.; Mulder, D. J.; Kuhl, T. L.; Mays, J. *Rev. Sci. Instrum.* **2008**, *79* (10), 103908.
(18) Smith, G. S.; Kuhl, T. L.; Hamilton, W. A.; Mulder, D. J.; Satija, S. *Physica B: Condensed Matter* **2006**, *385−386* (Part 1), 700–702.
(19) de Vos, W. M.; Biesheuvel, P. M.; de Keizer, A.; Kleijn, J. M.; Cohen Stuart, M. A. *Langmuir* **2008**, *24* (13), 6575–6584.
(20) de Vos, W. M.; Biesheuvel, P. M.; de Keizer, A.; Kleijn, J. M.; Cohen Stuart, M. A. *Langmuir* **2009**, *25* (16), 9252–9261.
(21) Grest, G. S. *J. Chem. Phys.* **1996**, *105* (13), 5532–5541.
(22) Murat, M.; Grest, G. S. *Macromolecules* **1989**, *22* (10), 4054–4059.
(23) Lai, P. Y.; Zhulina, E. B. *Macromolecules* **1992**, *25* (20), 5201–5207.
(24) Lai, P.-Y.; Binder, K. *J. Chem. Phys.* **1992**, *97* (1), 586–595.
(25) Lai, P.-Y.; Binder, K. *J. Chem. Phys.* **1993**, *98* (3), 2366–2375.
(26) Neelov, I. M.; Binder, K. *Macromol. Theory Simul.* **1995**, *4* (1), 119–136.
(27) Neelov, I. M.; Borisov, O. V.; Binder, K. *Macromol. Theory Simul.* **1998**, *7* (1), 141–156.
(28) Neelov, I. M.; Borisov, O. V.; Binder, K. *J. Chem. Phys.* **1998**, *108* (16), 6973–6988.
(29) He, G.-L.; Merlitz, H.; Sommer, J.-U.; Wu, C.-X. *Macromolecules* **2007**, *40* (18), 6721–6730.
(30) Coluzza, I.; Hansen, J.-P. *Phys. Rev. Lett.* **2008**, *100*, 016104.
(31) Seidel, C.; Netz, R. R. *Macromolecules* **2000**, *33* (2), 634–640.
(32) Kreer, T.; Metzger, S.; Muller, M.; Binder, K.; Baschnagel, J. *J. Chem. Phys.* **2004**, *120* (8), 4012–4023.
(33) Dimitrov, D. I.; Milchev, A.; Binder, K. *J. Chem. Phys.* **2006**, *125* (3), 034905.
(34) Dimitrov, D. I.; Milchev, A.; Binder, K. *J. Chem. Phys.* **2007**, *127* (8), 084905.
(35) von Werne, T.; Patten, T. E. *J. Am. Chem. Soc.* **2001**, *123* (31), 7497–7505.
(36) Ell, J. R.; Mulder, D. E.; Faller, R.; Patten, T. E.; Kuhl, T. L. *Macromolecules* **2009**, *42* (24), 9523–9527.
(37) Marrink, S. J.; de Vries, A. H.; Mark, A. E. *J. Phys. Chem. B* **2004**, *108* (2), 750–760.

(38) Hatakeyama, M.; Faller, R. *Phys. Chem. Chem. Phys.* **2007**, *9* (33), 4662–4672.
(39) Elliott, I. G.; Mulder, D. E.; Traskelin, P. T.; Ell, J. R.; Patten, T. E.; Kuhl, T. L.; Faller, R. *Soft Matter* **2009**, *5* (23), 4612–4622.
(40) Humphrey, W.; Dalke, A.; Schulten, K. *J. Mol. Graphics* **1996**, *14* (1), 33–38.
(41) Lindahl, E.; Hess, B.; van der Spoel, D. *J. Mol. Model.* **2001**, *7* (8), 306–317.
(42) Hess, B.; Kutzner, C.; van der Spoel, D.; Lindahl, E. *J. Chem. Theory Comput.* **2008**, *4* (3), 435–447.
(43) Berendsen, H. J. C.; Postma, J. P. M.; van Gunsteren, W. F.; DiNola, A.; Haak, J. R. *J. Chem. Phys.* **1984**, *81* (8), 3684–3690.
(44) de Vlieg, J.; Berendsen, H. J. C.; van Gunsteren, W. F. *Proteins: Struct., Funct., Genetics* **1989**, *6* (2), 104–127.
(45) Yamamoto, S.; Ejaz, M.; Tsujii, Y.; Fukuda, T. *Macromolecules* **2000**, *33* (15), 5608–5612.
(46) Whitmore, M. D.; Baranowski, R. *Macromol. Theory Simul.* **2005**, *14* (2), 75–95.
(47) Baranowski, R.; Whitmore, M. D. *J. Chem. Phys.* **1998**, *108* (23), 9885–9892.
(48) Chen, C. M.; Fwu, Y. A. *Phys. Rev. E* **2000**, *63*, 011506.
(49) Chakrabarti, A.; Toral, R. *Macromolecules* **1990**, *23* (7), 2016–2021.
(50) Grest, G. S.; Murat, M. *Macromolecules* **1993**, *26* (12), 3108–3117.
(51) Kent, M. S. *Macromol. Rapid Commun.* **2000**, *21* (6), 243–270.
(52) Baranowski, R.; Whitmore, M. D. *J. Chem. Phys.* **1995**, *103* (6), 2343–2353.
(53) Merlitz, H.; He, G.-L.; Wu, C.-X.; Sommer, J.-U. *Macromolecules* **2008**, *41* (13), 5070–5072.